

# Dalton Transactions

Accepted Manuscript



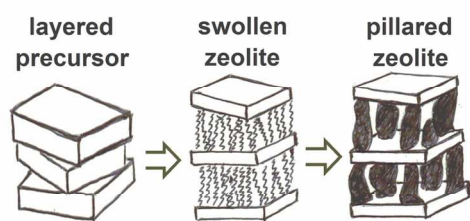
This is an *Accepted Manuscript*, which has been through the Royal Society of Chemistry peer review process and has been accepted for publication.

*Accepted Manuscripts* are published online shortly after acceptance, before technical editing, formatting and proof reading. Using this free service, authors can make their results available to the community, in citable form, before we publish the edited article. We will replace this *Accepted Manuscript* with the edited and formatted *Advance Article* as soon as it is available.

You can find more information about *Accepted Manuscripts* in the [Information for Authors](#).

Please note that technical editing may introduce minor changes to the text and/or graphics, which may alter content. The journal's standard [Terms & Conditions](#) and the [Ethical guidelines](#) still apply. In no event shall the Royal Society of Chemistry be held responsible for any errors or omissions in this *Accepted Manuscript* or any consequences arising from the use of any information it contains.

Porous structure of pillared zeolites IPC-3PI and MCM-36 depends in the lower mesopore region on the stacking of MWW layers.



145x108mm (300 x 300 DPI)

## High-resolution adsorption analysis of pillared zeolites IPC-3PI and MCM-36

Arnošt Zúkal\* and Martin Kubů

*Department of Synthesis and Catalysis, J. Heyrovský Institute of Physical Chemistry of the ASCR, v.v.i., Academy of Sciences of the Czech Republic, Dolejšková 2155/3, 182 23 Prague, Czech Republic. E-mail: arnost.zukal@jh-inst.cas.cz; Fax: +420 286 582 307; Tel.: +420 266 053 935*

Porous structure of pillared zeolites IPC-3PI and MCM-36 and their precursors IPC-3P and MCM-22P, respectively, has been investigated by means of a high-resolution adsorption analysis. The analysis was based on argon adsorption isotherms measured at 87 K from the relative pressure of  $10^{-6}$ . The isotherms were processed by means of  $t$ -plot method, which made possible to distinguish adsorption in micropores and adsorption in mesopores. Pore size distribution was evaluated from argon isotherms using Non-Local Density Functional Theory. Obtained results have shown that the microporous structure of the MWW layers is preserved in both pillared zeolites. In contrast to precursors IPC-3P and MCM-22P pillared samples are characterized by the formation of porous structure belonging to the lower mesopore region. The distribution of mesopores in zeolite IPC-3PI is broader and shifted to larger widths in comparison with the zeolite MCM-36.

## Introduction

Zeolites are widely applied in industry for adsorption, separation and catalysis. Their success can be attributed to the presence of micropores with well-defined structures and acidity of the framework. Nevertheless, the presence of micropores limits in many cases the performance of zeolite materials. The size of channels in three-dimensional (3D) zeolite frameworks, in practice below about 1 nm, restricts the accessibility of internal surface of channels for bulky molecules.<sup>1</sup> To overcome this disadvantage, different synthetic procedures were investigated. Higher accessible internal surface can be achieved by decreasing crystal size,<sup>2-4</sup> preparation of zeolites with larger pores<sup>5,6</sup> or by formation of thin zeolite layers.<sup>7</sup> Synthesis of so-called two-dimensional (2D) zeolites from layered precursors which are swollen and pillared has afforded combined microporous-mesoporous materials with enhanced surface areas.<sup>8,9</sup> Based on the layered precursor MCM-22P, a MCM-36 molecular sieve was produced.<sup>10</sup> The precursor MCM-22P was swollen at elevated temperature in solution of cationic long-chain surfactant in the hydroxide form or in the mixture of its halide salt with a tetraalkylammonium base under high pH. Prepared material was converted into product with siliceous pillars by treatment with tetraethyl orthosilicate (TEOS) followed by hydrolysis of TEOS. In analogy to this synthesis, the hydrolysis was also performed with solutions of  $\text{AlCl}_3\text{-NaOH}$  or  $\text{MgO/BaO-AlCl}_3\text{-NaOH}$  to prepare materials with aluminum-based binary oxides.<sup>11</sup>

Recently, a new pillared zeolitic material IPC-3PI was prepared from novel layered (two-dimensional) precursor IPC-3P.<sup>12</sup> The precursor was obtained as an intermediate during the synthesis of TUN zeolite at shorter synthesis time. In accordance to the Ostwald rule the precursor IPC-3P represents the least stable phase crystallizing first. (At a longer synthesis time, 3D zeolite TUN can be prepared as the final product of the synthesis.) To prepare

pillared material, the precursor IPC-3P was treated similarly as precursor MCM-22P in solution of hydroxide form of cationic long-chain surfactant. Swollen material IPC-3SW was converted using TEOS into pillared product IPC-3PI.

To describe the porous structure of IPC-3PI and MCM-36 zeolites and precursors IPC-3P and MCM-22P, the series of experimental techniques including gas adsorption was applied.<sup>10-19</sup> Adsorption of different gases was studied only under standard analysis conditions, which are insufficient to completely analyze microporous-mesoporous structures. For detailed analysis of these structures it is necessary to know the course of the adsorption isotherm in the whole region of pore filling, *i.e.* from the smallest amounts adsorbed to the amounts corresponding to completely filled pores. As physical adsorption of gases in microporous structures occurs in the region of relative pressures substantially lower than in the case of adsorption on mesoporous materials, the region of micropore filling spans several orders of magnitude beginning at relative pressure of  $10^{-7}$  -  $10^{-6}$ .

Nitrogen is generally accepted as the standard adsorptive for determination of surface areas and mesopore distributions using BET and BJH methods. However, the characterization of microporous structure of zeolites with nitrogen at temperature of its normal boiling point (77.36 K) is difficult.<sup>20</sup> The filling of zeolitic micropores with nitrogen takes place at relative pressures from  $10^{-7}$  to  $10^{-3}$ , where the rate of diffusion and adsorption equilibration is very slow. This may cause under-equilibration of measured adsorption isotherms, which will give erroneous results of the micropore analysis. The cations in zeolites, structural defects or surface functional groups give rise specific adsorption sites; the quadrupole moment of nitrogen molecule interacts with them. Therefore, nitrogen probes energetic heterogeneity of microporous materials and its adsorption is much more sensitive to the details of the structure of micropore walls.

In contrast to nitrogen, argon as an adsorptive at temperature of its normal boiling point (87.30 K) fills micropores at higher relative pressures from  $10^{-6}$  to  $10^{-2}$ , leading to accelerated diffusion and equilibration processes and also to a better precision of measurement.<sup>20</sup> Argon is considered not to interact with different heterogeneities of the microporous network. In general, argon at 87.30 K is always a better molecular probe than nitrogen since it does not give rise to specific interactions with a variety of specific adsorption sites.<sup>21</sup> For example nitrogen isotherms on MFI zeolite are shifted to lower pressures due to increasing concentration of silanol groups or amount of Al sites. On the other hand, the argon isotherms are independent on the amount of silanol and Al sites.<sup>22</sup> Hence the true textural characteristics of microporous materials can be evaluated from the argon adsorption data.

In this contribution, pillared zeolites IPC-3PI and MCM-36 and their precursors have been investigated. To characterize these materials, X-ray diffraction patterns and nitrogen isotherms at 77 K were recorded. The high-resolution adsorption analysis was performed using argon adsorption isotherms at 87 K measured from the relative pressure of  $10^{-6}$ . The argon adsorption data were processed firstly by means of *t*-plot method. After that, corresponding pore size distributions were evaluated using Non-Local Density Functional Theory (NLDFT).

## Experimental section

### Synthesis

Since the synthesis of 2D zeolite IPC-3PI from the new precursor IPC-3P was reported only recently,<sup>12</sup> the preparation of this material is described in greater details. The zeolite MCM-36 investigated in this paper was prepared following synthesis protocol given in Ref.<sup>16</sup> based

on the procedure reported in 1995 (see Ref.<sup>10</sup>). For this reason, synthesis of MCM-36 is described only briefly.

The lamellar precursor IPC-3P is formed initially during the synthesis of zeolite TNU-9 with 1,4-bis(N-methylpyrrolidinium)butane (1,4-MPB) and Na<sup>+</sup> ions as structure directing agents.<sup>23</sup> The synthesis of this material was performed in 500-mL Teflon-lined stainless steel autoclave heated at 433 K under agitation and autogenous pressure for 5 days. The solid product was filtered off, washed out with excess of distilled water and dried in the oven at 353 K overnight. This sample is denoted IPC-3P.

Swelling of IPC-3P was performed in 100 mL flask in which 3 g of dried IPC-3P was mixed with 60 mL of cetyltrimethyl ammonium hydroxide (CTMA-OH, obtained by ion exchange with AG1-X8 resin, BioRad) and the solution was stirred for 24 h at room temperature. After swelling, the mixture was centrifuged for 15 min followed by three-fold washing with distilled water and centrifugation for another 15 min. Finally, the solids were dried overnight in the oven at 333 K. The obtained dried sample was denoted IPC-3SW.

The swollen material was treated with tetraethyl orthosilicate (TEOS, 98 %, Aldrich) for 18 h at 358 K under reflux using 30 mL of TEOS per 1 g of the swollen sample. The solids were separated by centrifugation and dried in air at 313 K overnight. To ensure complete hydrolysis of TEOS, the powder was treated with water (200 mL/1 g of the sample) for 1 day. The product was centrifuged, washed with water and dried at 333 K. The obtained material was marked IPC-3PI.

The zeolite MCM-22P was synthesized using Ludox LS-30 and solid sodium aluminate as sources of silicon and aluminum, respectively. Hexamethyleneimine was employed as a structure directing agent. The hydrothermal synthesis was carried out at 423 K for 5 day; the product was isolated by centrifugation following by washing and drying.

MCM-36 was prepared similarly as IPC-3PI, *i.e.* by using cetyltrimethyl ammonium hydroxide for swelling and tetraethyl orthosilicate for pillaring.

Before adsorption measurements, all samples were calcined in a stream of air at 813 K for 8 h with a heating rate 1 K/min. After calcination the samples were treated four-times with 1 M  $\text{NH}_4\text{NO}_3$  solution (99%, Lach-Ner) for 4 h at room temperature using 100 mL of solution per 1 g of sample. (Calcined samples IPC-3P and MCM-22P are coded IPC-3 and MCM-22, respectively.)

## Methods

The structure and crystallinity of all samples was examined by X-ray powder diffraction (XRD) using a Bruker AXS D8 Advance diffractometer equipped with a graphite monochromator and position sensitive detector Vântec-1 using  $\text{CuK}\alpha$  radiation in Bragg-Bretano geometry.

Adsorption measurements were performed with an ASAP 2020 (Micromeritics, United States) volumetric instrument. In order to achieve necessary accuracy in the accumulation of adsorption data in a wide range of pressures, the instrument was equipped with three pressure transducers (13.3 Pa, 1.33 kPa and 133 kPa). The fresh zeolite samples were degassed starting at an ambient temperature up to 383 K (temperature ramp of  $0.5 \text{ K min}^{-1}$ ) until the residual pressure of 1 Pa was attained. After further heating at 383 K for 1 h, the temperature was increased up to 573 K (temperature ramp of  $1 \text{ K min}^{-1}$ ). At this temperature, degassing continued under the turbomolecular pump vacuum for 6 h. Adsorption isotherms of nitrogen at 77.3 K and argon at 87.3 K were recorded using liquid bath of  $\text{N}_2$  or Ar. Because helium penetrates deep into the micropores and takes a long time to diffuse from the zeolite particles, argon adsorption isotherms were measured on each sample two times. First

adsorption/desorption isotherm was measured in the region of relative pressures from 0.01 to 0.99. After that, the sample was evacuated directly on the sample port at 573 K for 2 h using turbomolecular pump to prevent an influence of residual helium on the shape of isotherm at the lowest equilibrium pressures. The following measurement of adsorption isotherm was performed in the region of relative pressures from *ca*  $10^{-6}$  to 0.6. In this case the sample was not exposed to helium because entered values of the free space volume were taken from the first measurement.

## Results and discussion

XRD patterns of the layered precursors IPC-3P and MCM-22P and their calcined forms are shown in Figure 1. All the materials are characterized by relatively sharp and well-defined maxima at  $2\theta = 7.1, 25$  and  $26^\circ$ , corresponding to the (100), (220) and (320) reflections of the MWW layers. The XRD patterns were discussed in the Ref.<sup>12</sup>; in this paper was suggested that the MWW layers in the IPC-3P are not vertically aligned as the MWW layers in the MCM-22P. (Suggested different stacking of MWW layers in both zeolites is schematically shown in Figure 2.) The conclusion concerning disordered stacking of MWW layers in the *c* axis observed by XRD is not generally accepted. Ref.<sup>9</sup> and references therein question that XRD is an adequate physical technique to detect such differences. Therefore, the high-resolution adsorption analysis of materials under study is useful because it can give more insight into the structure and properties of pillared zeolites.

XRD patterns of samples IPC-3PI and MCM-36 are shown in Figure 3. The patterns are qualitatively similar in the range of  $2\theta = 5-40^\circ$ . The interlayer peaks in the low-angle region correspond to layer spacing of 4.90 nm and 4.33 nm for IPC-3PI and MCM-36, respectively.

Nitrogen isotherms on calcined samples IPC-3, IPC-3SW, IPC-3PI, MCM-22 and MCM-36 are displayed in Figure 4. Surface areas  $S_{\text{BET}}$  of samples IPC-3, IPC-3SW and MCM-22 were calculated using adsorption data in the range of relative pressures from 0.07 to 0.18. Adsorption data in the range of relative pressures 0.05 - 0.12 were used for calculation of  $S_{\text{BET}}$  for samples IPC-3PI and MCM-36. Evaluated surface areas are listed in Table 1. It should be noted that surface area  $S_{\text{BET}}$  is frequently used for a comparison of different microporous/mesoporous materials although in this case the application of BET method is not quite correct due to presence of micropores. Isotherms on samples IPC-3PI and MCM-36 show an increase in the adsorbed amount at relative pressures between 0.05 and 0.30. Similar increase in the amount adsorbed was observed with isotherms on MCM-41 mesoporous molecular sieves due to filling of pores with diameter of 2.5 – 3.0 nm.<sup>24,25</sup> The similarity with isotherms on mesoporous molecular sieves and high values of surface area (642 m<sup>2</sup>/g and 586 m<sup>2</sup>/g for IPC-3PI and MCM-36, respectively) indicate the formation of new mesoporous structure in samples IPC-3PI and MCM-36 owing to swelling and pillaring.

Precursors IPC-3P and MCM-22P crystallize as aggregates of thin sheets which are preserved upon calcination.<sup>12,26</sup> Due to nitrogen condensation in interlayer voids in these aggregates, all isotherms yield narrow hysteresis loops. The volume  $V_{\text{BJH}}$  and diameter  $D_{\text{BJH}}$  of the interstitial voids determined from desorption branch of the hysteresis loops are given in Table 1. Because the hysteresis loops and parameters  $V_{\text{BJH}}$  and  $D_{\text{BJH}}$  are similar for all samples, it can be concluded that the swelling and pillaring practically do not change the interlayer voids.

According to the XRD and nitrogen adsorption data, the structure of materials under investigation appears to be as follows:

- The precursors IPC-3P and MCM-22P consist of MWW layers.

- The layer spacing of pillared materials IPC-3PI and MCM-36 increases to 4.90 nm and 4.33 nm for IPC-3PI and MCM-36, respectively.
- A new porous structure belonging to the lower mesopore region is formed in pillared samples while the interstitial voids among the particles are practically unchanged.

In order to gain more complete information on the porous structure of zeolites under study, argon adsorption was investigated. The use of argon is advantageous because this adsorptive does not give rise to specific interactions with different specific adsorption sites.<sup>21</sup> In order to achieve a high resolution, argon isotherms were measured at 87 K from the relative pressure  $p/p_s$  of  $\sim 10^{-6}$ . The isotherms in linear coordinates are shown in Figure 5. To show the low pressure region, the argon isotherms are displayed in semi-logarithmic coordinates in Figure 6. The inspection of these data reveals that isotherms of calcined samples IPC-3SW and IPC-3PI are almost identical at the relative pressure  $p/p_s < 10^{-2}$ . The isotherms on zeolites IPC-3 and MCM-22 are in this region slightly shifted to the higher amounts adsorbed in comparison with IPC-3PI and MCM-36; this difference can be explained by the formation of 3D structure during calcination of precursors IPC-3P and MCM-22P. Argon isotherms are qualitatively similar to the nitrogen isotherms at relative pressure higher than 0.05.

The first step of the analysis of argon adsorption data was based on the utilization of the  $t$ -plot method.<sup>27</sup> The choice of the reference isotherm, *i.e.* the dependence of the statistical thickness  $t$  on the relative pressure  $p/p_s$  for a reference material, is important for the correct application of the  $t$ -plot method.<sup>28</sup> In the case of investigated zeolites, the argon isotherm on non-porous silica with flat open surface seems the most suitable reference isotherm. Therefore, to transform argon adsorption data into the  $t$ -plot, the reference isotherm (Figure 7) evaluated from the data on LiChrospher Si-1000 Silica (EM Separations, Gibbstown, NJ,

US) was used.<sup>29</sup> In the region of the lowest equilibrium pressures it was completed with the data on Davisil Silica (Grace Davison Discovery Sciences, Lokeren, Belgium).<sup>30</sup>

The  $t$  values were interpolated by polynomial procedure for the series of  $\log p/p_0$  -5.5, -5.4, -5.3, ... , -0.1. The isotherm on investigated sample was interpolated for the same series of  $\log p/p_0$ . The  $t$ -plot, *i.e.* the dependence of amount adsorbed  $a$  on the thickness  $t$  was then constructed for corresponding values of  $p/p_0$ .

The  $t$ -plots for samples IPC-3 and IPC-3PI are shown in Figure 8. (The parts of isotherms corresponding to capillary condensation in interstitial voids were not transformed.) The almost vertical part for  $t < 0.05$  corresponds to the filling of micropores of the MWW layers. In the case of IPC-3 the subsequent linear part of the  $t$ -plot corresponds to the adsorption on the outer surface of zeolite particles. In the case of IPC-3PI the steeper linear part of the  $t$ -plot corresponds not only to adsorption on the original surface of zeolite particles but also to completed filling of the mesopores formed by calcination of swollen and pillared materials. The argon condensation in these mesopores gives rise to a swing of  $t$ -plot in the interval of  $t$  from 0.5 to 0.6.<sup>31</sup> It should be noted that similar effect was observed in the case of argon adsorption on MFI nanosheets.<sup>32</sup> Due to a short distance between MFI sheets a condensation of argon occurs which can be distinguished from adsorption in the zeolite framework.

The linear part of  $t$ -plot can be expressed as  $a = A + B t$ , where  $a$  is amount adsorbed and  $A$  and  $B$  are constants. The intercept  $A$  is equivalent to the adsorption capacity of micropores.<sup>31</sup> Based on this parameter, it is possible to calculate micropore volume under assumption that the adsorbed argon has a bulk-like liquid density. However, this assumption is questionable for the adsorbate confined in zeolite micropores because the densities of the adsorbed states are not equivalent to those of the condensed liquids.<sup>33</sup> Therefore, the volume of micropores is estimated here using NLDFT approach. The slope  $B$  is equivalent to the

surface area of mesopores; this surface area  $S_{t\text{-plot}} = 1.375 B$ . (The coefficient 1.375 was evaluated from constants given in Ref.<sup>29</sup>.)

Similar  $t$ -plots were obtained for the pair MCM-22 and MCM-36 (Figure 9) and for the sample IPC-3SW (not shown). Evaluated parameters  $A$ ,  $B$ , and  $S_{t\text{-plot}}$  are listed in Table 1. An inspection of Table 1 reveals that the micropore capacity of samples IPC-3PI and MCM-36 is *ca* 85 % of micropore capacity of calcined precursors. On the other hand, the surface area  $S_{t\text{-plot}}$  of pillared samples is considerably higher and it attains 288 – 299 m<sup>2</sup>/g. The decrease in the micropore capacity can be explained by the presence of pillars from amorphous silica without micropores, the increase in the surface area clearly takes place due to adsorption on the inner surface of mesopores formed by the swelling. The texture parameters determined for the sample IPC-3SW (Table 1) show that it contains mesopores as sample IPC-3PI; however, the volume of mesopores is smaller in comparison with pillared sample.

The application of  $t$ -plot enables to distinguish the adsorption in micropores and adsorption in mesopores, which is important for determination of pore size distribution. From it follows that calculated pore sizes distributions are not deformed due to simultaneous adsorption in both pore groups. The amount  $a_{MI}$  adsorbed in micropores is given by the difference  $(a - B t)$ . The dependences of  $a_{MI}$  vs.  $t$  in Figures 8 and 9 show that at  $t < 0.1$  (*i.e.* at  $p/p_0 < 0.01$ ) the term  $B t$  is negligible; hence, adsorption of argon at low relative pressure occurs practically only in micropores. On the other hand, at  $t > 0.3$  (*i.e.* at  $p/p_0 > 0.1$ )  $a_{MI}$  is constant, *i.e.* due to completely filled micropores adsorption takes place only in mesopores.

In the second step of the analysis of argon adsorption, the pore size distributions (PSD) of all samples were calculated from argon isotherms by the NLDFT model for cylindrical pores in H exchanged zeolites. The application of NLDFT has enabled us to calculate pore size distribution in the lower mesopore region. The interval of relative pressure for calculations performed using Micromeritics software spans values from  $p/p_0 \sim 10^{-6}$  to  $p/p_0$

~0.6. Evaluated PSD curves displayed in Figure 10 show two distinct pore groups. (As described in the caption, the Figure 10 consists of two parts for clarity.) The distribution of the first group of micropores is centered at the pore width  $w \sim 0.56$  nm. It evidences that the MWW microporous structure is preserved in all samples. The micropore volume (Table 1) of pillared materials IPC-3PI and MCM-36 determined by the DFT method is 85 % and 90 %, respectively, of the micropore volume of samples IPC-3 and MCM-22. Since the pillars are formed from amorphous silica, all the micropores are present only in the MWW layers. Therefore, the decrease in the micropore volume of samples IPC-3PI and MCM-36 takes place due to pillaring with 10 – 15 wt. % of amorphous silica. It should be noted that the micropore volumes of pillared materials determined in the Ref.<sup>12</sup> from nitrogen isotherm using the  $t$ -plot method were smaller than data in Table 1. The values obtained by the DFT method from argon isotherms seem more realistic.

In contrast to the mesopores formed by interstitial voids, the second group of pores belongs to lower mesopore region. The mesopore volume  $V_{ME}$  increases from 0.104 cm<sup>3</sup>/g for the IPC-3SW to 0.169 cm<sup>3</sup>/g for the IPC-3PI; for MCM-36 the mesopore volume of 0.138 cm<sup>3</sup>/g is slightly lower than that of IPC-3PI (Table 1). The mesopore size distribution curves for samples IPC-3SW, IPC-3PI and MCM-36 shown in Figure 10 are centered at 3.1 nm, 3.0 nm and 2.8 nm, respectively. The decrease in these values corresponds to the decrease in the interlayer spacing from 4.9 nm to 4.3 nm determined for IPC-3PI and MCM-36, respectively. As the thickness of MWW layers is 2.5 nm,<sup>8</sup> the differences between the layer spacing and layer thickness are with all samples somewhat smaller than the values corresponding to the center of mesopore distribution. We speculate that this problem is connected with the shape of mesopores formed between pillars. Although the X-ray patterns of IPC-3PI and MCM-36 are similar, it can be supposed that possible misaligned stacking of MWW layers in the

zeolites IPC-3P, IPC-3SW and IPC-3PI gives rise to the broader mesopore distribution in IPC-3PI.

## Conclusions

High-resolution adsorption analysis represents a complementary approach to the X-ray diffraction method for evaluation of texture properties of 2D zeolites. Based on the argon adsorption data measured at 87 K from the relative pressure of  $10^{-6}$ , the textural parameters inaccessible by means of X-ray diffraction were determined. The isotherms were processed by means of *t*-plot method with the argon isotherm on non-porous silica used as the reference. The application of *t*-plot made possible to distinguish adsorption in micropores and adsorption in mesopores, which is important for determination of pore size distribution. PSD curves evaluated using the NLDFT model for cylindrical pores in H exchanged zeolites show two distinct groups of micropores and mesopores. The microporous structure of the MWW layers was preserved in all materials. The mesoporous structures of zeolites IPC-3PI and MCM-36 formed by pillaring belong to the lower mesopore region. The PSD curves reveal that the distribution of mesopores the IPC-3PI zeolite is broader than that in MCM-36 zeolite.

## Acknowledgement

AZ thanks the Micromeritics Instrument Corporation for a support in the frame of the Instrument Grant Program while MK acknowledges the Czech Science Foundation (project 13-17593P).

## References

- 1 J. Čejka, G. Centi, J. Perez-Pariente and W. J. Roth, *Catal. Today*, 2012, **179**, 2.
- 2 M. Choi, K. Na, J. Kim, Y. Sakamoto, O. Terasaki and R. Ryoo, *Nature*, 2009, **461**, 246.
- 3 L. Bonetto, M. A. Camblor, A. Corma and J. Perez-Pariente, *Appl. Catal. A*, 1992, **82**, 37.
- 4 A. Corma, V. Fornes, S. B. Pergher, T. L. M. Maesen and J. G. Burglass, *Nature*, 1998, **396**, 353.
- 5 A. Corma, M. J. Diaz-Cabanas, J. Jiang, M. Afeworki, D. L. Dorset, S. L. Soled and K. G. Strohmaier, *Proc. Natl. Acad. Sci. U.S.A.*, 2010, **107**, 13997.
- 6 C. Martínez and A. Corma, *Coord. Chem. Rev.*, 2011, **255**, 1558.
- 7 W. J. Roth, P. Nachtigall, R. E. Morris and J. Čejka, *Chem. Rev.*, 2014, in press.
- 8 W. J. Roth, *Stud. Surf. Sci. Catal.*, 2007, **168**, 222.
- 9 F. S. O. Ramos, M. K. de Pietre and H. O. Pastore, *RSC Adv.*, 2013, **3**, 2084.
- 10 W. J. Roth, C. T. Kresge, J. C. Vartuli, M. E. Leonowicz, A. S. Fung and S. B. McCullen, *Stud. Surf. Sci. Catal.*, 1995, **94**, 301.
- 11 J.-O. Barth, A. Jentys, J. Kornatowski and J. A. Lercher, *Chem. Mater.*, 2004, **16**, 724.
- 12 M. Kubů, W. J. Roth, H. F. Greer, W. Zhou, R. M. Morris, J. Přeč and J. Čejka, *Chem. Eur. J.*, 2013, **19**, 13937.
- 13 Y. J. He, G. S. Nivarthi, F. Eder, K. Seshan and J. A. Lercher, *Microporous Mesoporous Mater.* 1998, **25**, 207.
- 14 J.-O. Barth, J. Kornatowski and J. A. Lercher, *J. Mater. Chem.*, 2002, **12**, 369.
- 15 J. Kornatowski, J.-O. Barth, K. Erdmann and M. Rozwadowski, *Microporous Mesoporous Mater.*, 2006, **90**, 251.
- 16 W. J. Roth, O. V. Shvets, M. Shamzhy, P. Chlubná, M. Kubů, P. Nachtigall and J. Čejka, *J. Am. Chem. Soc.*, 2011, **133**, 6130.
- 17 P. Chlubná, W. J. Roth, A. Zukał, M. Kubů and J. Pavlatová, *Catal. Today*, 2012, **179**, 35.
- 18 P. Chlubná, W. J. Roth, H. Greer, W. Zhou, O. Shvets, A. Zukał, J. Čejka and R. E. Morris, *Chem. Mater.*, 2013, **25**, 542.

- 19 W. J. Roth, P. Nachtigall, R. E. Morris, P. S. Wheatley, V. R. Seymour, S. E. Ashbrook, P. Chlubná, L. Grajciar, M. Položij, A. Zukal, O. Shvets and J. Čejka, *Nat. Chem.*, 2013, **5**, 628.
- 20 M. Thommes, *Stud. Surf. Sci. Catal.*, 2007, 168, 495.
- 21 J. Landers, G. Yu. Gor and A. V. Neimark, *Colloids Surf. A: Physicochem. Eng. Aspects*, 2013, <http://dx.doi.org/10.1016/j.colsurfa.2013.01.007>.
- 22 K. Nakai, J. Sonoda, M. Yoshida, M. Hakuman and H. Naono, *Adsorption*, 2007, **13**, 351.
- 23 S. B. Hong, H. K. Min, Ch. H. Shin, P. A. Cox, S. J. Warrender and P. A. Wright, *J. Am. Chem. Soc.*, 2007, **129**, 10870.
- 24 M. Kruk and M. Jaroniec, *J. Phys. Chem. B*, 1997, **101**, 583.
- 25 A. Zukal, M. Thommes and J. Čejka, *Microporous Mesoporous Mater.*, 2007, **104**, 52.
- 26 J. Pawlesa, A. Zukal and J. Čejka, *Adsorption*, 2007, **13**, 257.
- 27 B. C. Lippens and J. H. de Boer, *J. Catal.*, 1965, **4**, 319.
- 28 J. Rathousky, A. Zukal, N. Jaeger and G. Schulz-Ekloff, *J. Chem. Soc. Faraday Trans.*, 1992, **88**, 489.
- 29 M. Kruk and M. Jaroniec, *Chem. Mater.*, 2000, 12, 222.
- 30 A. Zukal, unpublished results.
- 31 S. Lowell, J. E. Shields, M. A. Thomas and M. Thommes, *Characterization of Porous Solids and Powders: Surface Area, Pore size and Density*, Kluwer, Dordrecht, The Netherlands, 2004, p. 132, 139.
- 32 S. K. Schnell, L. Wu, A. J. J. Koekkoek, S. Kjestrup, E. J. M. Hensen and T. J. H. Vlught, *J. Phys. Chem. C*, 2013, **117**, 24503.
- 33 E. Maglara, A. Pullen, D. Sullivan and W. C. Conner, *Langmuir*, 1994, **10**, 4167.

### List of figures

**Fig 1** XRD patterns of the layered precursors IPC-3P and MCM-22P and their calcined forms IPC-3 and MCM-22.

**Fig 2** The stacking of the MWW layers in IPC-3P and MCM-22P precursors.

**Fig 3** XRD patterns of pillared samples IPC-3PI and MCM-36.

**Fig 4** Nitrogen adsorption isotherms at 77 K on calcined samples IPC-3, IPC-3SW, IPC-3PI, MCM-22 and MCM-36.

**Fig 5** Argon adsorption isotherms at 87 K on calcined samples IPC-3, IPC-3SW, IPC-3PI, MCM-22 and MCM-36 in linear coordinates.

**Fig 6** Argon adsorption isotherms at 87 K on calcined samples IPC-3, IPC-3SW, IPC-PI, MCM-22 and MCM-36 in semi-logarithmic coordinates.

**Fig 7** Argon adsorption isotherm at 87 K on LiChrospher Si-1000 Silica (blue points) and Davisil Silica (red points) in linear and semi-logarithmic coordinates.

**Fig 8** The  $t$ -plots for samples IPC-3 and IPC-3PI. Linear fits of  $t$ -plot are displayed by solid or dashed straight lines. Calculated isotherms of argon adsorption in micropores of MWW layers are denoted by symbols  $\oplus$  (IPC-3PI) or  $\otimes$  (IPC-3).

**Fig 9** The  $t$ -plots for samples MCM-22 and MCM-36. Linear fits of  $t$ -plot are displayed by solid or dashed straight lines. Calculated isotherms of argon adsorption in micropores of MWW layers are denoted by symbols  $\oplus$  (MCM-36) or  $\otimes$  (MCM-22).

**Fig 10** Pore size distribution curves for samples IPC-3PI, IPC-3, IPC-3SW, MCM-36 and MCM-22. Left side of the figure displays the micropore distribution in MWW layers, right side shows the distribution of mesopores formed by swelling and pillaring.

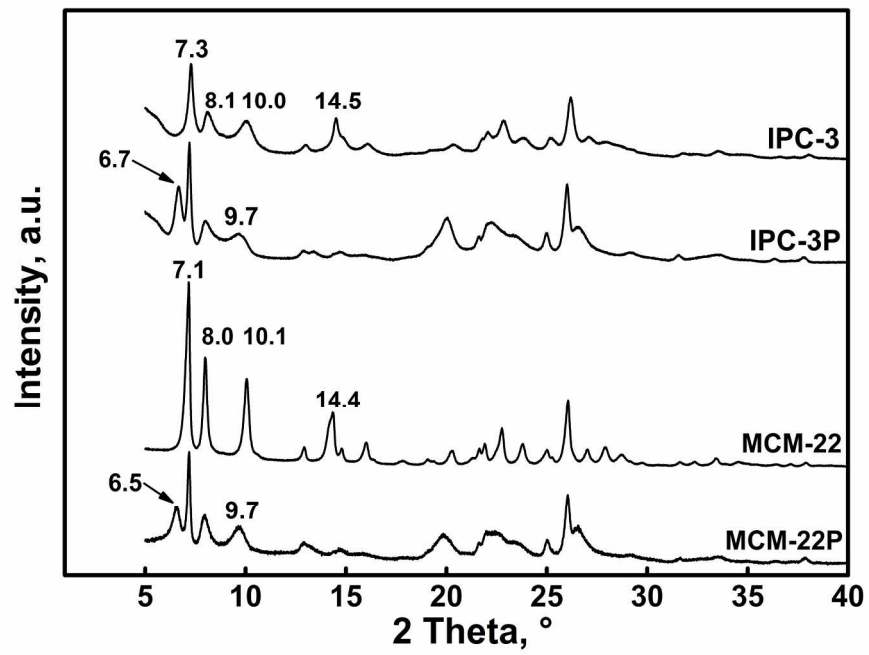
### List of tables

**Table 1** Characteristics of samples under study based on nitrogen and argon adsorption isotherms

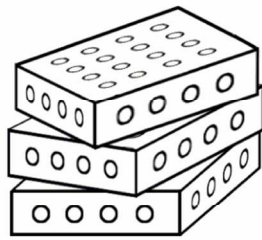
**Table 1** Characteristics of samples under study based on nitrogen and argon adsorption isotherms

Sample	Nitrogen			Argon				
	$S_{\text{BET}}$ m <sup>2</sup> /g	$V_{\text{BJH}}$ cm <sup>3</sup> /g	$D_{\text{BJH}}$ (nm)	$A$ cm <sup>3</sup> STP/g	$B$ cm <sup>3</sup> STP/g.nm	$S_{\text{t-plot}}$ m <sup>2</sup> /g	$V_{\text{MI}}^*$ cm <sup>3</sup> /g	$V_{\text{ME}}^*$ cm <sup>3</sup> /g
IPC-3	452.1	0.24	5-10	99.7	74.0	101.7	0.190	0.035
IPC-3SW	532.0	0.30	4-10	91.8	136.8	188.1	0.171	0.104
IPC-3PI	642.0	0.28	5-8	85.2	209.6	288.2	0.160	0.169
MCM-22	483.0	0.26	4-10	103.0	95.8	131.7	0.200	0.070
MCM-36	586.4	0.26	4-8	89.7	217.6	299.2	0.180	0.138

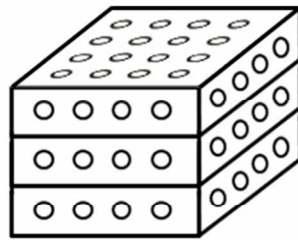
(\*) The micropore and mesopore volumes were determined using NLDFT method.



215x173mm (300 x 300 DPI)

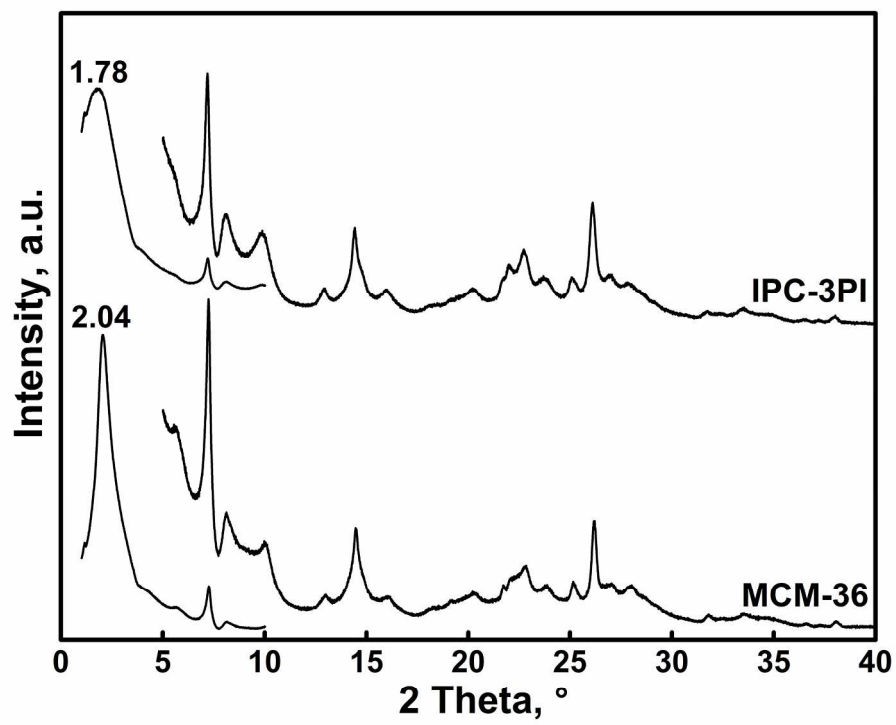


**IPC-3P**

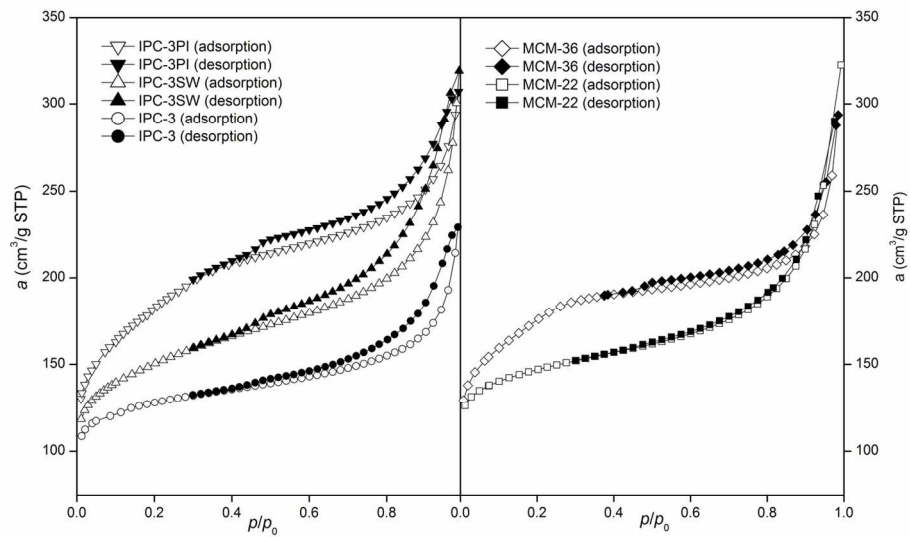


**MCM-22P**

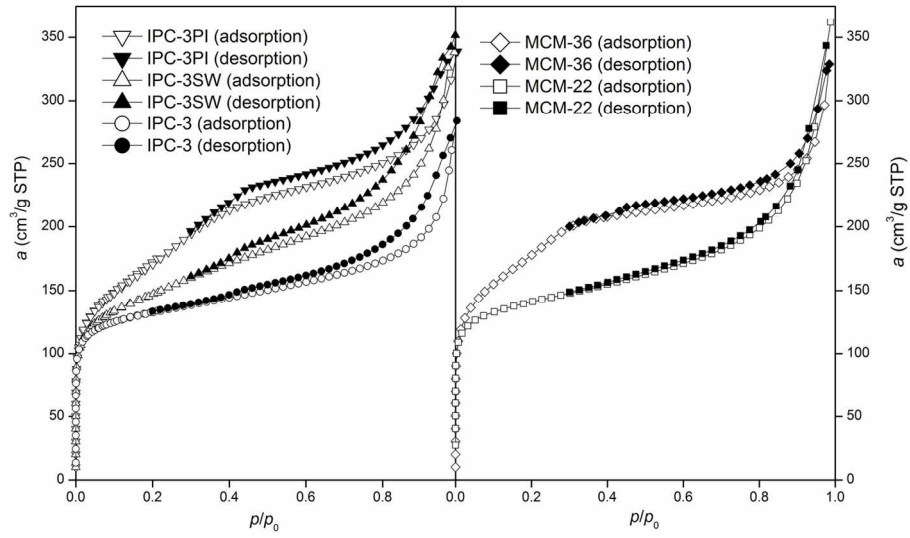
176x148mm (300 x 300 DPI)



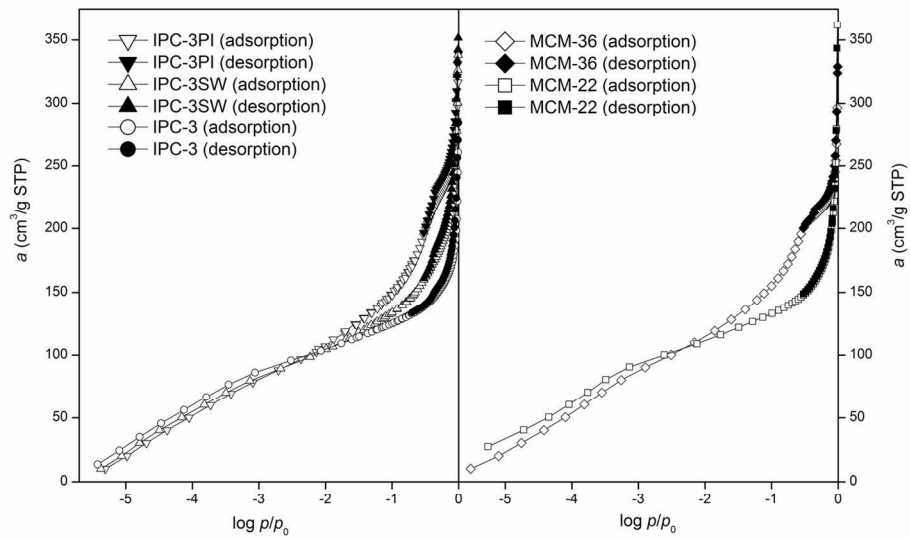
219x194mm (300 x 300 DPI)



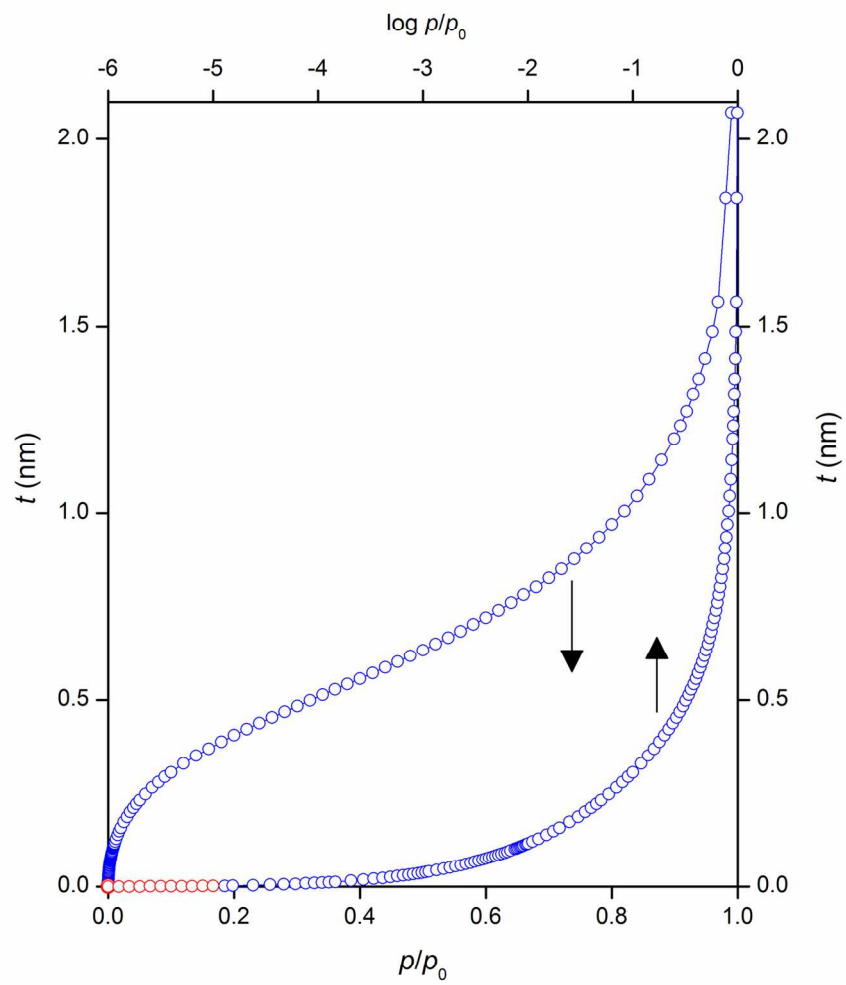
136x89mm (300 x 300 DPI)



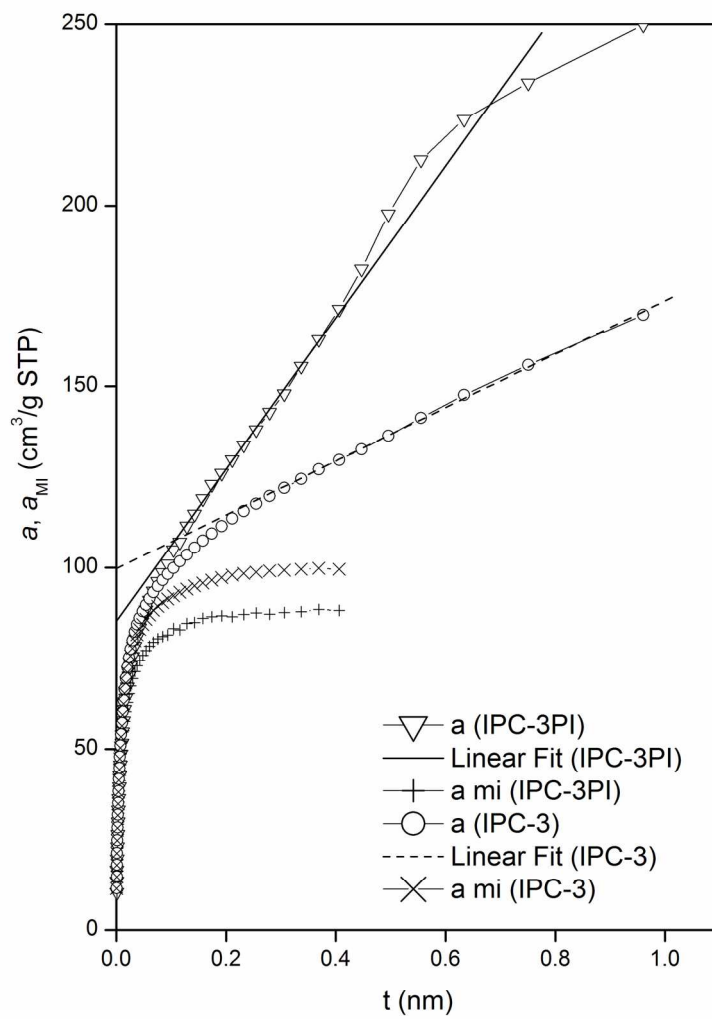
139x91mm (300 x 300 DPI)



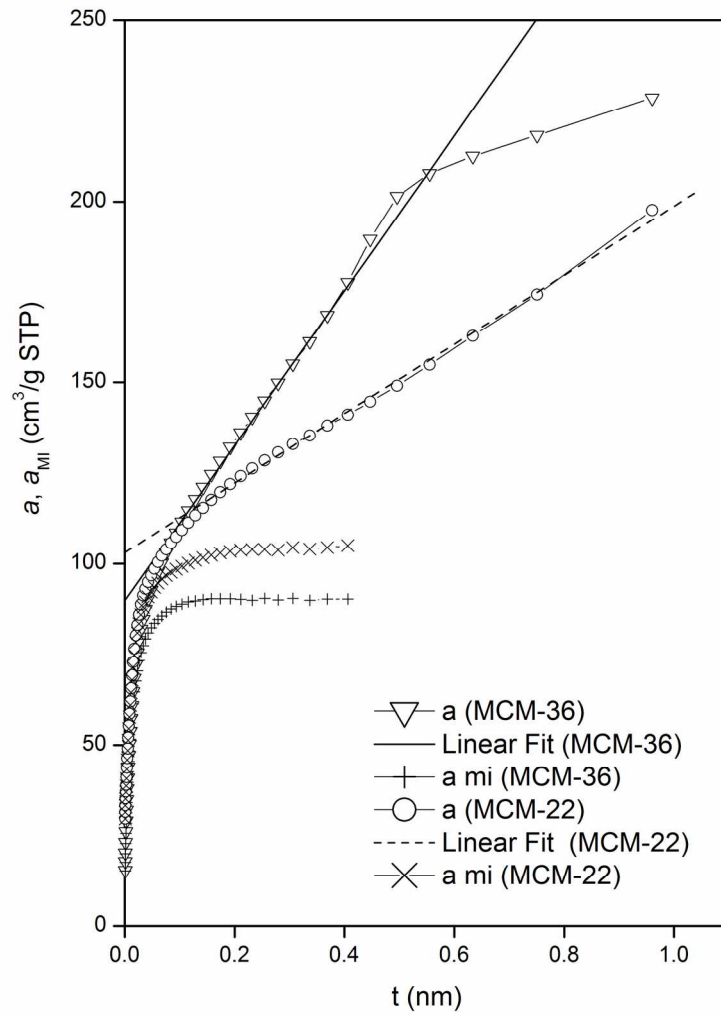
139x92mm (300 x 300 DPI)



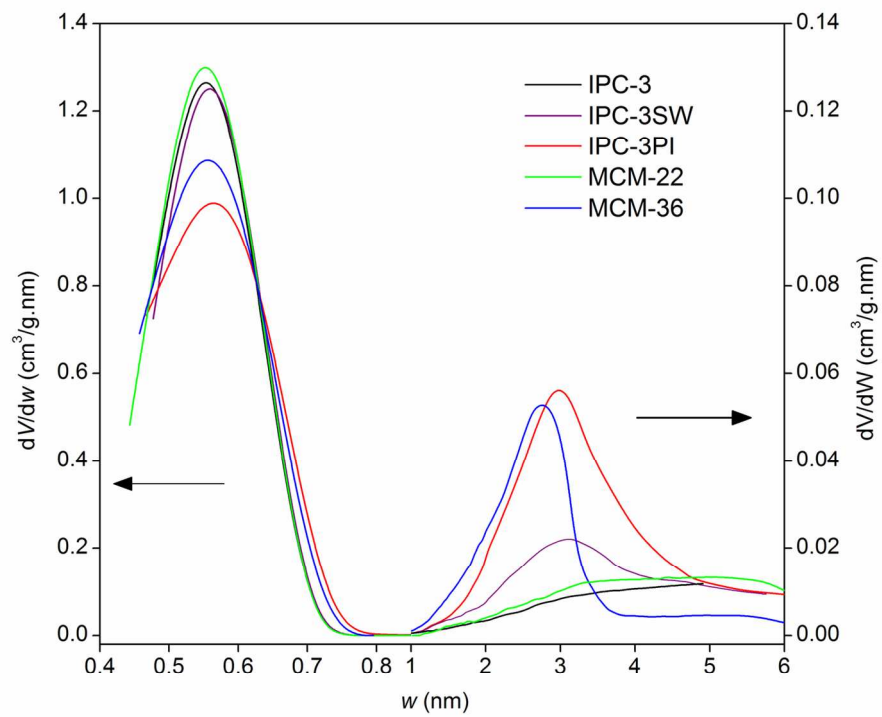
145x166mm (300 x 300 DPI)



159x207mm (300 x 300 DPI)



159x206mm (300 x 300 DPI)



137x117mm (300 x 300 DPI)